# Interaction-induced atomic displacements revealed by drift-corrected dynamic force spectroscopy

Shigeki Kawai,* Thilo Glatzel, Sascha Koch, Alexis Baratoff, and Ernst Meyer
*Department of Physics, University of Basel, Klingelbergstrasse 82, CH-4056 Basel, Switzerland*
(Received 2 November 2010; revised manuscript received 20 December 2010; published 24 January 2011)

The three-dimensional force field above an NaCl(001) surface was measured on a fine grid by small amplitude dynamic force spectroscopy at room temperature. After careful drift corrections, maps in nominally equivalent symmetry planes as well as in sections parallel to the surface reveal distance-dependent shifts of characteristic atomic-sized features. These shifts reflect asymmetries of the probing tip apex but are mainly due to atomic displacements induced by short-range forces. In addition, weak decaying force oscillations with a period close to the interlayer spacing are detected at distances where no atomic-scale variations are expected. Stronger site-dependent changes appear in the interaction-induced energy dissipation.

DOI: 10.1103/PhysRevB.83.035421 PACS number(s): 68.37.Ps, 07.79.Lh, 34.20.Cf

## I. INTRODUCTION

Interactions of surfaces with adsorbed molecules, clusters, and scanning probe tips are at the focus of numerous on-going investigations. Evidence from experiments as well as numerical simulations indicates, for instance, that technologically relevant phenomena, such as friction and wear are ultimately due to the formation and rupture of contacts of various sizes down to the nanometer scale.[1] Dynamic force microscopy (DFM) has proven to be a very sensitive technique for detecting interaction forces between an atomically sharp tip and a sample surface[2,3] via the resonance frequency shift of an oscillating cantilever.[4] DFM topographic images are usually obtained by adjusting the tip-sample distance to keep a constant frequency shift. The latter is affected by forces, which vary over distances smaller than the imposed oscillation amplitude, while atomic-scale contrasts are mainly due to short-range interactions with typical decay lengths on the order of 100 pm. The interpretation of the observed DFM contrast is not straightforward because changes in the amplitude and/or the structure and chemical constitutions of the tip apex can drastically change the relative contributions of short- and long-range forces.[5] Since the tip apex condition is often not well defined, the reproducibility of quantitative measurements with different tips is low, except in special cases where the contrast is dominated by a single species firmly attached to the apex, e.g., by intentional manipulation.[6,7]

Extraction of the force perpendicular to the surface from frequency shifts measured as a function of the tip-sample distance $Z$, so-called dynamic force spectroscopy (DFS), facilitates comparison with numerical simulations.[8,9] Since the first such quantitative comparison above specific atomic sites,[5] this technique has become a very powerful tool.[10,11] Even a clear discrimination of short-range interactions with different surface species has been demonstrated.[6,7]

Sequential DFS measurements at equally spaced lateral distances have been performed on flat surfaces.[12–16] Such data can provide additional information about tip-sample interactions, e.g., the interaction potential as well as parallel force components.[14,17,18] Thus, the potential well trapping a single adsorbed atom and the lateral force needed to move it to an adjacent lattice site could be determined.[15] Until now, high-resolution measurements of the three-dimensional (3D) force field have been demonstrated only at low temperature (LT).[7,12,15,19] One notable exception is the 3D DFS room temperature (RT) measurement of adsorbed molecules in solution achieved in 53 s using a dedicated setup and custom-made electronics.[20] Since the measurement time drastically increases when a large number of grid points is used, thermal drift and the creep of the scanner usually affect such 3D DFS measurements even at LT.[12] Albers *et al.* used a tomographic approach based on a sequence of topographic images recorded at spaced tip-sample distances, weakly controlled by a frequency shift.[19] The corresponding 3D dataset was *analyzed after aligning characteristic features* in the $Z$ direction. Observed lateral shifts and distortions of maxima and minima between images can, however, arise from atomic displacements induced by tip-sample interactions, especially at close distances. As shown by atomistic simulations, in particular, on NaCl(001),[21] reversible displacements, vertical as well as lateral, can affect the force field and may be difficult to distinguish from drift and creep artifacts. At RT, vibrational anharmonicity enhances these displacements, while thermal activation smears atomic jumps[22] so that stronger apparently continuous lateral shifts can occur.[13] Moreover, nonlinear drift and creep can create distortions during the long capture time for each image, thus, making the tomographic approach questionable unless such artifacts are systematically eliminated.

We present high-resolution drift-corrected 3D DFS measurements on NaCl(001) at RT. Two-dimensional (2D) cuts, both perpendicular and parallel to the surface, clearly reveal significant shifts of characteristic features, which can be attributed to atom displacements, besides tip apex asymmetry. We also tentatively explain the origin of weak slowly decaying site-dependent force oscillations with a period comparable to the interlayer spacing, which are unexpectedly observed at larger distances.

## II. EXPERIMENTAL

All experiments were performed with our in-house DFM, operating at RT in ultrahigh vacuum (UHV).[23] A clean NaCl(001) surface was obtained by cleaving in UHV and then annealed at 300 °C to remove residual charges caused by cleavage. The second flexural resonance mode of a commercially available Si cantilever (Nanosensor NCL-PPP)

 

was used to sense vertical tip-sample interaction forces.[24–26] The high effective stiffness $k_{2nd}$ permits stable small amplitude operation with improved sensitivity.[27,28] The oscillation amplitude $A_{2nd}$ was kept constant at 400 pm with an automatic gain controller.[4] The value $k_{2nd} = 1450$ N/m was determined via bimodal DFS using the same amplitudes for the first and second flexural resonance modes ($A_{1st} = A_{2nd} = 10$ nm).[29] Before starting the DFS measurements, the cantilever was annealed at 150 °C in the preparation chamber. The tip was cleaned by $Ar^+$ sputtering, then gently contacted to the sample surface without any oscillation in order to pick up an NaCl cluster, and scanned for several hours to stabilize the cluster.

Figure 1(a) shows a DFM topographic image of NaCl(001) in an area of $1.4 \times 1.4$ nm$^2$, which obtained a constant frequency shift of the second mode $\Delta f_{2nd} = -170$ Hz. The $X$ and $Y$ directions join adjacent maxima, and the $Z$ direction is perpendicular to the image plane. The array of dots indicates the positions of $71 \times 71$ grid points at which individual DFS measurements were performed at 256 equally spaced $Z$ points over a 1-nm interval.

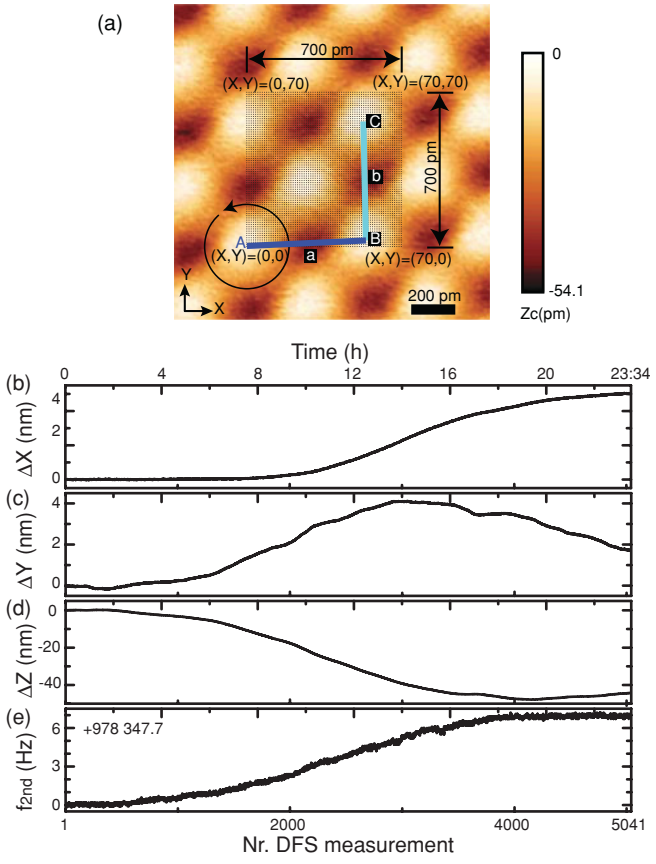


FIG. 1. (Color online) (a) DFM topographic image of NaCl(001) for $\Delta f_{2nd} = -170$ Hz in an area of $1.4 \times 1.4$ nm$^2$. The superposed array of dots depicts the positions of DFS measurements. The positions of the maxima are indicated as A, B, and C, and those of the minima are indicated as a and b. Drifts of the (b) $X$, (c) $Y$, and (d) $Z$ relative tip-sample position measured by atom tracking, and of (e) the resonance frequency of the second flexural mode $f_{2nd}$ during the entire 3D measurement versus the number of each DFS measurement, i.e., as a function of time. The $X$, $Y$, and $Z$ directions are defined. Operation parameters: $A_{2nd} = 400$ pm, $V_{bias} = 0$ V. $f_{2nd} = 978\,354$ Hz, $Q_{2nd} = 6400$, and $k_{2nd} = 1450$ nm.

Ambient temperature fluctuations in the microscope chamber cause thermal drifts even after the average temperature has stabilized. Since a high-resolution 3D DFS measurement takes a relatively long time, drift artifacts must be monitored and eliminated as much as possible. In a short-term single DFS measurement, the drift rate can be regarded as constant, and the drift can then be compensated by applying linear voltages to three orthogonal $X,Y,Z$ piezoscanners.[30] However, this method cannot be applied to a long-term measurement due to the nonlinear evolution of the thermal drift. In this paper, we readjusted the relative tip-sample position between each single DFS measurement by atom tracking[11,31] above a particular maximum of the essentially undistorted topographic image [Fig. 1(a)], which was recorded before the DFS measurements. Thus, drifts of the relative $(X,Y,Z)$ tip-sample position were compensated by readjusting the sample position so that the maximum at $(X,Y) = (0,0)$ remained there, while the tip-sample distance was controlled by setting $\Delta f_{2nd} = -170$ Hz. Henceforth, this position defines the *origin of the closest approach distance* $Z_c$ in one oscillation cycle. The required $X,Y,Z$ adjustments averaged over 6 s were recorded together with the *thermal shift* of the second flexural mode resonance frequency $f_{2nd}$ measured at $Z_c = 1.5$ nm above the atom-tracked position. The time-averaged cantilever deflection shifted the $Z_c = 0$ origin by only $-4$ pm.[25] Owing to the thermal properties of Si around RT, $f_{2nd}$ can significantly be shifted by ambient temperature fluctuations over the total measurement time. Unless it is compensated, this shift affects $\Delta f_{2nd}$, hence, the strength of the tip-sample force close to the surface and results in a slow modulation of the feedback controlled $Z_c$. Therefore, this shifted resonance frequency was reset to be the reference frequency with respect to how the desired *interaction-induced* shift $\Delta f_{2nd}$ is determined by a phase-locked loop prior to each subsequent DFS measurement. The necessary control steps were performed using external control software for scanning probe microscopy and spectroscopy (Nanonis SC4/RC4) and atom tracking (Nanonis AT4). The recorded drifts of the relative tip-sample $X,Y,Z$ coordinates and of $f_{2nd}$ during the entire 3D DFS measurement time of 23 h and 34 min are shown in Figs. 1(b)–1(e). The maximum excursions in the $X$, $Y$, and $Z$ directions were 51, 4.3, and 48 nm, respectively. At the start, the measured $f_{2nd}$ was 978 347.7 Hz , and its maximum shift was +7.4 Hz. The temperature in the measurement chamber is, to a certain extent, influenced by the external RT. Based on the negative thermal coefficient of $f_{2nd}$ ($\approx -50$ Hz/K at RT[2]), the temperature of the system presumably decreased only by approximately 0.15 C. The variations of the observed drifts appear strongly correlated with each other, except in the slow-scan $Y$ direction. Anyway, for high-resolution 3D DFS measurements, the drift must be small enough because a residual effect remains even if most of the $Z$ drift is compensated by assuming that the drift rate is constant during each DFS measurement. The $Z$ drift was corrected by rescaling the $Z$ axis for each DFS measurement. A site-independent long-range DFS curve was measured separately and was connected to the 5041 short-range DFS curves for subsequent force extraction.

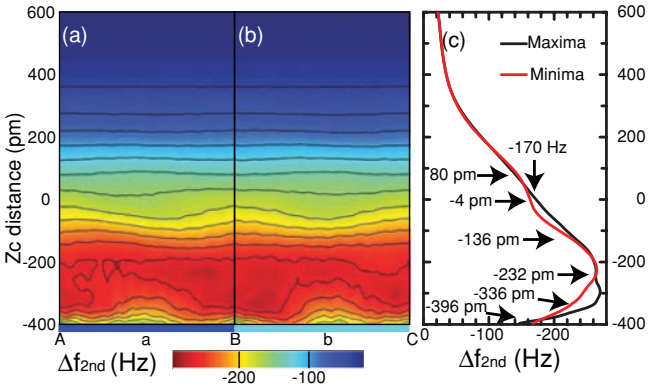


FIG. 2. (Color online) Two-dimensional maps constructed from the drift corrected $\Delta f_{2nd}(Z_c)$ along (a) A-B and (b) B-C in Fig. 1(a); (c) $\Delta f_{2nd}(Z_c)$ curves averaged over the maxima and minima in the image.

## III. RESULTS AND DISCUSSION

### A. Frequency shift

Figures 2(a) and 2(b) show 2D maps with contours of constant $\Delta f_{2nd}$ in two vertical planes passing through A-B and B-C in Fig. 1(a), respectively. Atomic contrast becomes observable below $Z_c \approx 100$ pm. The smoothness of the contours indicates that *no permanent* tip apex rearrangements occurred during the entire measurement. Well-defined maxima and minima develop between $Z_c \sim 0$ and about $-200$ pm . However, as indicated by the contours and clearly shown by the constant height maps in Fig. 3, these features shift up to almost $\pm a/2$ in $X$ and somewhat less in $Y$, $a = 564$ pm being the lattice spacing of NaCl. Below $Z_c \approx -300$ pm, well-defined maxima appear at (a and b), i.e., the contrast is inverted, whereas, the minima are strongly distorted. In both ranges, the well-defined features form a pattern consistent with the structure of the NaCl(001) surface. Nevertheless, although the planes of Figs. 2(a) and 2(b) are nominally equivalent, noticeable differences occur. Taken together, the above-mentioned shifts and deviations strongly suggest significant tip and/or sample deformations in both $X$ and $Y$ directions caused by tip-sample interactions. If the tip is terminated by an asymmetric NaCl cluster,[16,21,32] its apex preferably deforms in an off-symmetry direction. Figure 2(c) shows the average distance dependencies of $\Delta f_{2nd}$ at the positions of the maxima (A, B, and C) and minima (a and b) in the image. Both curves exhibit wiggles, in particular, around the most negative $\Delta f_{2nd}$, such as those observed in previous DFS measurements on NaCl(001).[13,16] Based on $T \to 0$ simulations, such features can be attributed to displacements of strongly interacting tip and sample ions. If the tip apex is represented by a cubic NaCl cluster with a ⟨111⟩ axis perpendicular to the surface, quite different displacements are predicted above surface cations and anions.[21] However, simulations, which consider less symmetric model tips, predict significant attraction at both sites,[16,32] as observed here. Moreover, ion displacements are then more similar and typically involve lateral components. Since our constant height maps exhibit no significant *relative shifts* of maxima versus minima, common shifts of up to $\pm a/2$ are most likely due to lateral deformations of the same order around the tip apex.

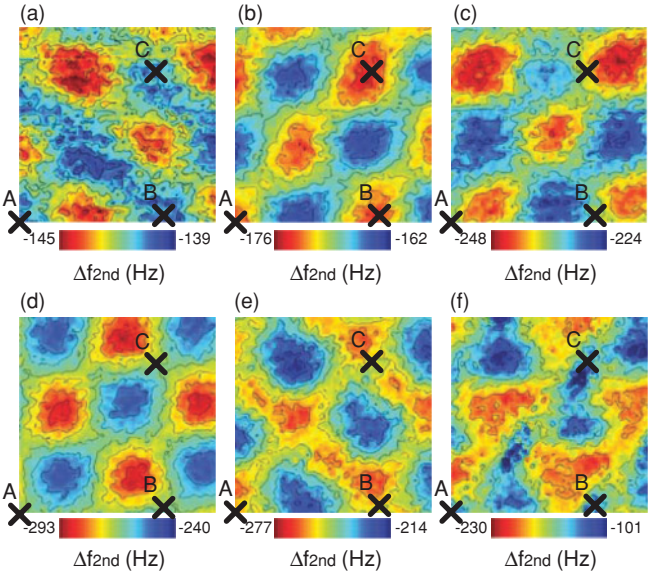


FIG. 3. (Color online) Constant height maps of the frequency shift $\Delta f_{2nd}$ maps at (a) $Z_c = 80$ pm, (b) $Z_c = -4$ pm, (c) $Z_c = -136$ pm, (d) $Z_c = -232$ pm, (e) $Z_c = -336$ pm, and (f) $Z_c = -396$ pm, constructed from the complete drift-corrected 3D dataset. Crosses indicate the positions of the maxima in Fig. 1(a).

One of the main advantages of high-resolution 3D DFS measurements is the possibility of constructing constant height maps, which allow visualizing contrast changes of measured quantities (interaction-induced frequency shift $\Delta f$ and energy dissipation $E_{ts}$) as well as derived ones (vertical force on the tip $F_{int}$, tip-sample interaction energy $U$, and lateral force components) at a series of closest approach distances $Z_c$. The construction of such constant height maps free of drift artifacts is rather challenging, especially at RT, except if the required data are sufficiently rapidly recorded. In most 3D DFS measurements, including ours, such data are composed of nonsequentially measured signals so that even small drifts of $Z_c$ can cause significant artifacts.

With the goal of better understanding how tip and sample deformations can affect the DFM contrast at different distances, 2D maps of the $\Delta f_{2nd}$ are shown in Fig. 3 for the six indicated values of $Z_c$. In order to facilitate the comparison with the previous discussion, these values are also indicated by horizontal arrows in Fig. 2(c). The crosses indicate the positions of the observed maxima $A, B, C$ at $Z_c = 0$ in the constant $\Delta f_{2nd}$ topographic image in Fig. 1(a). In the conventional imaging range where $d\Delta f_{2nd}/dZ > 0$, the $(X, Y)$ positions with the most negative $\Delta f_{2nd}$ in a constant height map at a certain $Z_c$ essentially correspond to maxima in a DFM topographic image at a constant $\Delta f_{2nd}$ equal to the average of $\Delta f_{2nd}$ over the constant height map. This is indeed observed for the map at $Z_c = -4$ pm in Fig. 3(b). Somewhat surprisingly, for $Z_c = 80$ pm [Fig. 3(a)], the most negative $\Delta f_{2nd}$ is observed almost midway between adjacent crosses. We surmise that this contrast inversion is a manifestation of the weak decaying oscillatory force discussed later in connection with Fig. 4(f). Between $Z_c = 24$ pm and about $-260$ pm, well-developed maxima and minima develop, as seen in Figs. 3(b)–3(d), but continuously shift laterally while the overall pattern remains consistent with the structure of

the NaCl(001) surface. Such shifts imply that the assignment of maxima and minima in a single seemingly undistorted topographic image or constant-height map to particular surface ions or atoms is, in general, questionable. This may be possible in a narrow range at a safe distance where no appreciable shifts and distortions occur, and the atomic-scale contrast is sufficiently clear, as around $Z_c = 0$. However, this safe imaging range is not known *a priori*. For $Z_c = -232$ pm [Fig. 3(d)], the variation of $\Delta f_{2nd}$ between maximum and minimum (least and most negative) values is much larger than could be surmised from Figs. 2(a)–2(c), owing to significant $X$ and $Y$ shifts away from the lines A-B and B-C, which join adjacent crosses in Fig. 3. Therefore, vertical 2D maps and, especially, single DFS measurements at positions of the maxima and minima in a single undistorted topographic image or constant-height map can be misleading. Complete information about actual 3D variations of the force field can only be obtained from a sufficiently dense set of drift-corrected DFS measurements or constant-height maps. Around $Z_c = -336$ pm, the areas with the most negative $\Delta f_{2nd}$ start to deform and partly merge. The maxima stop shifting and coincide with their positions for $-4$ pm, in agreement with the expectation that the least attractive force should occur above ions of the same polarity as the tip apex. Close to the bottom of the investigated range [Fig. 3(f)], the maxima also deform and split.

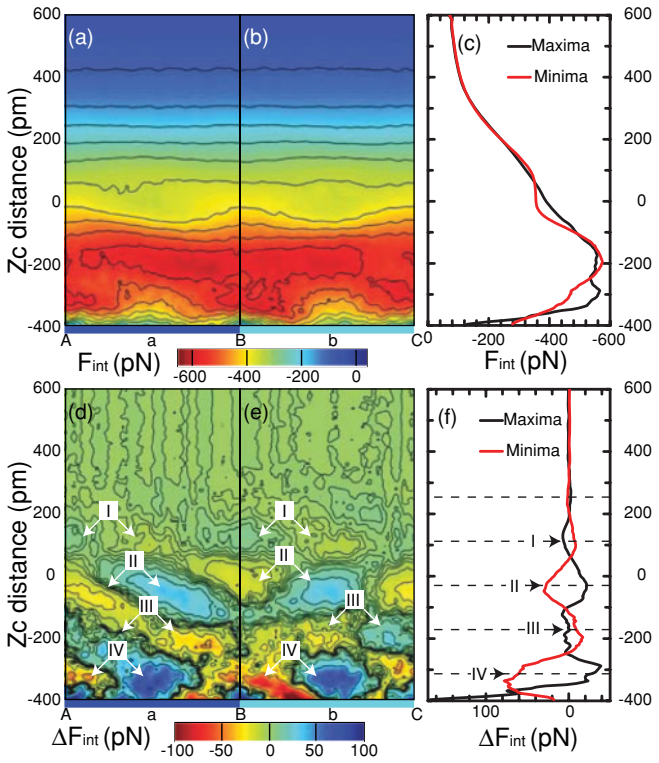


FIG. 4. (Color online) Two-dimensional maps of the interaction force $F_{int}$ extracted from the drift-corrected $\Delta f_{2nd}$ along (a) A-B and (b) B-C; (c) average distance dependence of $F_{int}$ at the maxima (A, B, and C) and the minima (a and b). Remainder $\Delta F_{int}$ after subtraction of the $(X,Y)$ averaged force at each $Z_c$ along (d) A-B and (e) B-C; (f) average distance dependence of $\Delta F_{int}$ at the maxima and the minima.

### B. Interaction force

When the tip apex comes close to the sample surface, displacements can become jumplike and can cause different forces during approach and retraction in one oscillation cycle. This results in a hysteresis loop and leads to energy dissipation.[22,33] In this situation, the even force $F_{int}$ extracted from the measured $\Delta f$ is the result of averaging over many oscillation cycles with distinct distance-dependent forces caused by atom jumps between tip and sample or by switching between different tip apex configurations with varying probabilities.[34] $F_{int}(Z)$ was extracted using the Sader-Jarvis algorithm.[9] Figures 4(a) and 4(b) show 2D $F_{int}$ maps in vertical planes through A-B and B-C in Fig. 1(a). For the chosen $A_{2nd}$, which is comparable to the half-width of the attractive force minimum, the distance dependencies of $F_{int}$ and $\Delta f_{2nd}$ are similar, and Figs. 4(a)–4(c) and Figs. 2(a)–2(c) show similar patterns. This is qualitatively expected because $A_{2nd} = 400$ pm lies between the limits of large and ultrasmall amplitudes (compared to the range of short-range forces) where $\Delta f/f$ is approximately proportional to $-\sqrt{(U F_{int})}$ and to $-dF_{int}/dZ$, respectively.[35]

In order to emphasize the site dependence of $F_{int}$, the common long-range contribution should preferably be determined and subtracted separately.[5,6] Because such a procedure proved unsatisfactory on NaCl(001),[16,21] the $(X,Y)$ average of $F_{int}$ was simply subtracted at each $Z_c$. The resulting short-range 2D $\Delta F_{int}$ force maps along A-B and B-C are shown in Figs. 4(d) and 4(e), respectively. For $Z_c > 200$ pm, no significant contrast is observed, but around $Z_c = 150$ pm (region I), weak variations of $\approx \pm 6$ pN become detectable. For $Z_c < 50$ pm, the contours become distorted due to strong tip-sample deformations. However, an alternating pattern of positive and negative $\Delta F_{int}$ is still observed. Figure 4(f) shows the resulting oscillatory $\Delta F_{int}(Z_c)$ curves averaged over the maxima and minima in Fig. 1(a). The observed oscillation becomes approximately sinusoidal with a decaying envelope for $Z_c > 0$. The period is surprisingly close to the bulk interlayer spacing $a/2 = 282$ pm, and the decay length is $\approx$130 pm. Since $F_{int}$ is still attractive at the bottom of Figs. 2(b) and 2(c), the surface layer is further below. The decaying oscillation of $\Delta F_{int}$ extends more than three to five interlayer spacings above the surface and cannot be caused by short-range interactions. We tentatively propose that this unexpected site-dependent force arises from a superposition of contributions induced by long-range forces in successive sample layers. Van der Waals attraction causes elastic deformations, whereas, the electric field due to the uncompensated tip-sample contact potential difference spreads out inside the insulating sample. On the atomic scale, those two kinds of long-range forces induce nearly parallel and opposite cation and anion displacements, respectively. The resulting deviations are enhanced under the tip but decrease in magnitude away from it, both perpendicular and parallel to the surface of the sample. Summing up contributions from discrete layers can give rise to the weak site-dependent decaying modulation of the long-range force. It is important to note that, in the case of *undistorted ordered layers*, the site-dependent part of any nominally long-range force arising from a superposition of pairwise power-law terms *decays exponentially without any oscillation* perpendicular

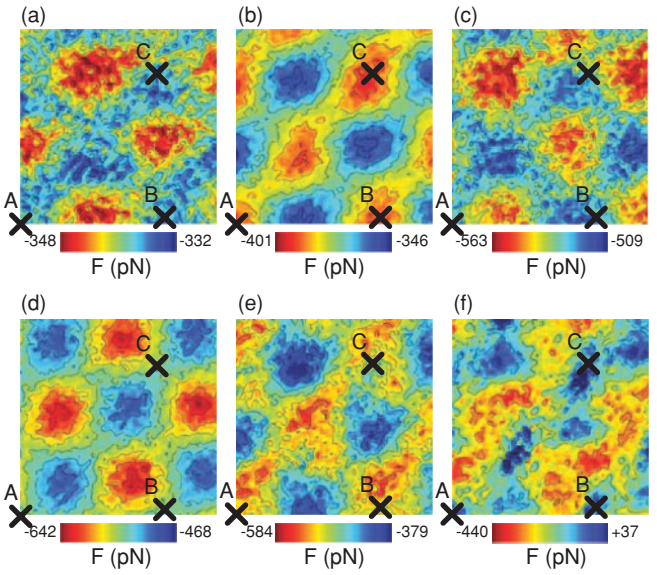


FIG. 5. (Color online) Constant-height maps of the vertical interaction force at (a) $Z_c = 80$ pm, (b) $Z_c = -4$ pm, (c) $Z_c = -136$ pm, (d) $Z_c = -232$ pm, (e) $Z_c = -336$ pm, and (f) $Z_c = -396$ pm, extracted from the complete drift-corrected 3D $\Delta f_{2nd}$ dataset. Crosses indicate the positions of the maxima in Fig. 1(a).

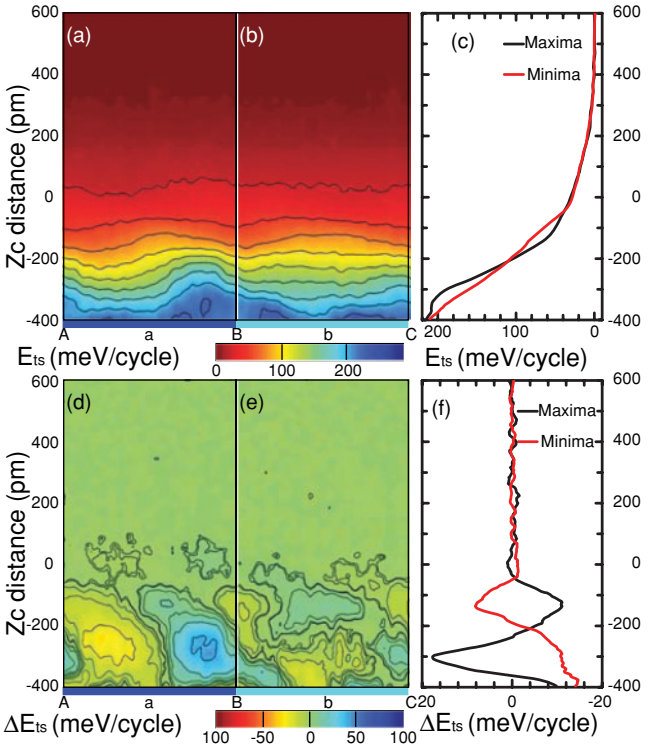


FIG. 6. (Color online) Two-dimensional maps of the drift-corrected energy dissipation $E_{ts}$ along (a) A-B and (b) B-C; (c) average distance dependencies of $E_{ts}$ at the maxima and minima. Remainder $\Delta E_{ts}$ after subtraction of the $(X,Y)$ averaged dissipation at each $Z_c$ along (d) A-B and (e) B-C; (f) average distance dependence of $\Delta E_{ts}$ at the maxima and the minima.

to the surface[36] with a decay length $a/(2\pi\sqrt{2}) = 63$ pm in the case of the lowest lateral Fourier component above a *rigid* NaCl(001) surface. The unambiguous experimental observation of the decaying oscillating $\Delta F_{int}$ appears to require the careful drift corrections and superior signal-to-noise ratio achieved in this paper. A theoretical verification of the proposed mechanism is desirable but would be challenging in view of the small magnitude of the effect and of the necessary multiscale modeling.

As already mentioned, variations similar to those of $\Delta f_{2nd}$ are found for $F_{int}$. A comparison of Fig. 3 with the constant-height maps in Fig. 5 confirms this trend. For this reason, the following discussion is focused on the origin of the distortions apparent in Figs. 3(e) and 3(f). Judging from the scale bars in Figs. 5(e) and 5(f), as well as Fig. 2(c), these phenomena happen where $F_{int}$ starts rising, thus, indicating a repulsive contribution. Nevertheless, attraction remains quite appreciable, except around maxima in Fig. 5(f). The variation of $F_{int}$ keeps growing with decreasing $Z_c$, however. Presumably, the tip apex gets trapped around minima of the resulting corrugated interaction energy landscape, and several tip atoms also significantly interact with the surface, thus, causing subsidiary energy minima within the channels, which join the crosses in that range.

### C. Energy dissipation

The interaction-induced energy dissipation per oscillation cycle $E_{ts}$ was calculated from the measured excitation amplitude $A_{exc}$ required to keep $A_{2nd}$ constant.[37] On resonance $E_{ts} \approx E_0(A_{exc}/A_{exc,0} - 1)$, $E_0 \cong \pi k_{2nd} A_{2nd}^2 / Q_{2nd}$ is the intrinsic cantilever energy loss per oscillation cycle, and $A_{exc,0}$ is the constant excitation amplitude at a sufficiently large distance. Figures 6(a) and 6(b) show 2D $E_{ts}$ maps along A-B and B-C, respectively. Comparing the average distance dependence at the maxima and minima shown in Fig. 6(c) with Fig. 4(c), one sees that, upon approach, $E_{ts}$ rises slowly, then more rapidly in the range where $F_{int}$ is most attractive and the strongest shifts occur, and finally tends to saturate. We attribute the small tail to joule heating and the remaining dependence to a force hysteresis loop with flanks broadened on average by thermal activation.[22] Although the sample is an insulator, lossy ac currents are induced in the oscillating doped Si tip by the finite electric field due to the uncompensated dc contact potential difference between tip and sample. Owing to the long-range nature of the macroscopic electric field, this contribution is site independent. On the other hand, force hysteresis caused by strong enough short-range forces leads to atomic-scale contrast in $E_{ts}$. To emphasize this site dependence, the $(X,Y)$-averaged $E_{ts}$ dataset was, similar to $F_{int}$, subtracted at each $Z_c$. The resulting 2D $\Delta E_{ts}$ maps along A-B and B-C are shown in Figs. 6(d) and 6(e). Compared to $F_{int}$ and $\Delta F_{int}$, the differences between $E_{ts}$ and $\Delta E_{ts}$ maps in symmetry-equivalent planes are stronger. This is consistent with earlier observations that contrast in $E_{ts}$ is more sensitive to tip rearrangements and, generally, to atoms with locally reduced coordination, which, being weakly bound, are preferentially destabilized.[38] This also implies reduced correlations between the positions of maxima and minima in $E_{ts}$ and those in $F_{int}$.

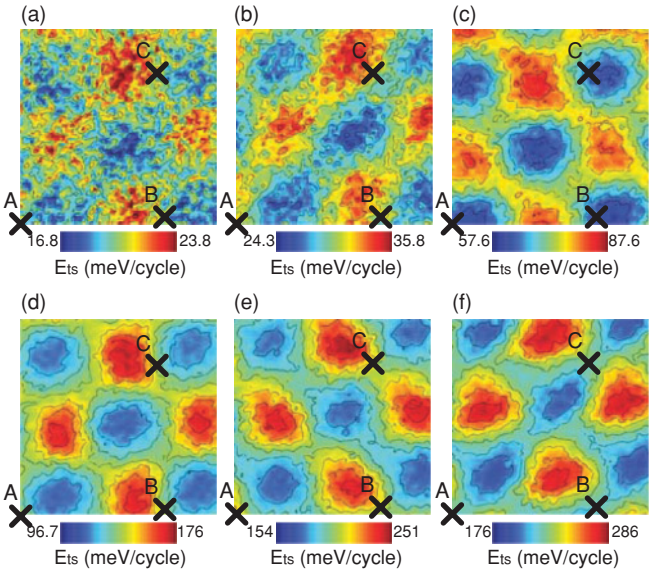


FIG. 7. (Color online) Constant-height maps of the average energy dissipation per cycle $E_{ts}$ at (a) $Z_c = 80$ pm, (b) $Z_c = -4$ pm, (c) $Z_c = -136$ pm, (d) $Z_c = -232$ pm, (e) $Z_c = -336$ pm, and (f) $Z_c = -396$ pm, constructed from the complete drift-corrected 3D dataset. Crosses indicate the positions of the maxima in Fig. 1(a).

Constant-height maps of the average energy dissipation per oscillation cycle constructed from drift-corrected data recorded simultaneously with $\Delta f_{2nd}$ are shown in Fig. 7 for the same six values of $Z_c$. Well-defined maxima and minima develop below $Z_c \sim -100$ pm, i.e., in the range where $E_{ts}$ is mainly due to force hysteresis caused by atom jumps. Maximum dissipation tends to occur around less negative [Figs. 7(d) and 7(e)] or positive [Fig. 7(f)] values of $F_{int}$, i.e., where a repulsive contribution to the force acts, in qualitative agreement with the destabilization of the foremost tip ion conjectured by Schirmeisen *et al.*[13] As mentioned earlier, this correlation is far from perfect, however, for the plausible reasons stated there.

## IV. CONCLUSIONS

In conclusion, our carefully drift-compensated high-resolution 3D RT measurements demonstrate that tip asymmetry and atomic displacements significantly distort the force field probed by the tip of a force microscope close to an atomically flat surface. Even stronger effects appear in the simultaneously recorded energy dissipation. A complete picture of the distortions can only be revealed by a sufficiently dense set of 3D measurements.

## ACKNOWLEDGMENTS

This work was supported, in part, by the ESF EUROCORE program FANAS, the Swiss National Science Foundation, and by the NCCR program Nanoscale Science of the Swiss National Science Foundation.

*shigeki.kawai@unibas.ch

[1] Y. Mo, K. T. Turner, and I. Szlufarska, Nature (London) **457**, 1116 (2009).
[2] F. J. Giessibl, Rev. Mod. Phys. **75**, 949 (2003).
[3] S. Morita, F. J. Giessibl, and R. Wiesendanger, *Noncontact Atomic Force Microscopy* (Springer, Berlin, 2009), Vol. 2.
[4] T. R. Albrecht, P. Grütter, D. Horne, and D. Rugar, J. Appl. Phys. **69**, 668 (1991).
[5] M. A. Lantz, H. J. Hug, R. Hoffmann, P. J. A. van Schendel, P. Kappenberger, S. Martin, A. Baratoff, and H. J. Güntherodt, Science **291**, 2580 (2001).
[6] Y. Sugimoto, P. Pou, M. Abe, P. Jelinek, R. Pérez, S. Morita, and O. Custance, Nature (London) **446**, 64 (2007).
[7] L. Gross, F. Mohn, N. Moll, P. Liljeroth, and G. Meyer, Science **325**, 1110 (2009).
[8] U. Dürig, Appl. Phys. Lett. **75**, 433 (1999).
[9] J. E. Sader and S. P. Jarvis, Appl. Phys. Lett. **84**, 1801 (2004).
[10] R. Hoffmann, L. N. Kantorovich, A. Baratoff, H. J. Hug, and H. J. Güntherodt, Phys. Rev. Lett. **92**, 146103 (2004).
[11] M. Abe, Y. Sugimoto, O. Custance, and S. Morita, Appl. Phys. Lett. **87**, 173503 (2005).
[12] H. Hölscher, S. M. Langkat, A. Schwarz, and R. Wiesendanger, Appl. Phys. Lett. **81**, 4428 (2002).
[13] A. Schirmeisen, D. Weiner, and H. Fuchs, Phys. Rev. Lett. **97**, 136101 (2006).
[14] K. Ruschmeier, A. Schirmeisen, and R. Hoffmann, Phys. Rev. Lett. **101**, 156102 (2008).
[15] M. Ternes, C. P. Lutz, C. F. Hirjibehedin, F. J. Giessibl, and A. J. Heinrich, Science **319**, 1066 (2008).
[16] R. Hoffmann, D. Weiner, A. Schirmeisen, and A. S. Foster, Phys. Rev. B **80**, 115426 (2009).
[17] A. Schwarz, H. Hölscher, S. M. Langkat, and R. Wiesendanger, AIP Conf. Proc. **696**, 68 (2003).
[18] Y. Sugimoto, T. Namikawa, K. Miki, M. Abe, and S. Morita, Phys. Rev. B **77**, 195424 (2008).
[19] B. J. Albers, T. C. Schwendemann, M. Z. Baykara, N. Pilet, M. Liebmann, E. I. Altman, and U. D. Schwarz, Nat. Nanotechnol. **4**, 307 (2009).
[20] T. Fukuma, Y. Ueda, S. Yoshioka, and H. Asakawa, Phys. Rev. Lett. **104**, 016101 (2010).
[21] M. A. Lantz, R. Hoffmann, A. S. Foster, A. Baratoff, H. J. Hug, H. R. Hidber, and H.-J. Güntherodt, Phys. Rev. B **74**, 245426 (2006).
[22] L. N. Kantorovich and T. Trevethan, Phys. Rev. Lett. **93**, 236102 (2004).
[23] L. Howald, E. Meyer, R. Lüthi, H. Haefke, R. Overney, H. Rudin, and H. J. Güntherodt, Appl. Phys. Lett. **63**, 117 (1993).
[24] S. Kawai, S. Kitamura, D. Kobayashi, S. Meguro, and H. Kawakatsu, Appl. Phys. Lett. **86**, 193107 (2005).
[25] S. Kawai, T. Glatzel, S. Koch, B. Such, A. Baratoff, and E. Meyer, Phys. Rev. B **80**, 085422 (2009).
[26] S. Kawai, F. Rose, T. Ishii, and H. Kawakatsu, J. Appl. Phys. **99**, 104312 (2006).
[27] F. J. Giessibl, H. Bielefeldt, S. Hembacher, and J. Mannhart, Appl. Surf. Sci. **140**, 352 (1999).

[28]S. Kawai and H. Kawakatsu, Appl. Phys. Lett. **89**, 023113 (2006).
[29]S. Kawai, T. Glatzel, S. Koch, B. Such, A. Baratoff, and E. Meyer, Phys. Rev. Lett. **103**, 220801 (2009).
[30]M. Abe, Y. Sugimoto, T. Namikawa, K. Morita, N. Oyabu, and S. Morita, Appl. Phys. Lett. **90**, 203103 (2007).
[31]D. W. Pohl and R. Möller, Rev. Sci. Instrum. **59**, 840 (1988).
[32]R. Oja and A. S. Foster, Nanotechnology **16**, S7 (2005).
[33]N. Sasaki and M. Tsukada, Jpn. J. Appl. Phys. **39**, L1334 (2000).
[34]S. A. Ghasemi, S. Goedecker, A. Baratoff, T. Lenosky, E. Meyer, and H. J. Hug, Phys. Rev. Lett. **100**, 236106 (2008).
[35]F. J. Giessibl and H. Bielefeldt, Phys. Rev. B **61**, 9968 (2000).
[36]W. A. Steele, Surf. Sci. **36**, 317 (1973).
[37]B. Anczykowski, B. Gotsmann, H. Fuchs, J. P. Cleveland, and V. B. Elings, Appl. Surf. Sci. **140**, 376 (1999).
[38]R. Bennewitz, A. S. Foster, L. N. Kantorovich, M. Bammerlin, C. Loppacher, S. Schär, M. Guggisberg, E. Meyer, and A. L. Shluger, Phys. Rev. B **62**, 2074 (2000).